

# Interactions of Heavy Hadrons using Regge Phenomenology and the Quark Gluon String Model

Y.R. de Boer<sup>a,b</sup>, A.B. Kaidalov<sup>a</sup>, D.A. Milstead<sup>c</sup>, O.I. Piskounova<sup>d</sup>

<sup>a</sup>*Institute for Theoretical and Experimental Physics, Moscow, Russia.*

<sup>b</sup>*University of Twente, Enschede, the Netherlands.*

<sup>c</sup>*Fysikum, Stockholms Universitet, Stockholm, Sweden.*

<sup>d</sup>*P.N.Lebedev Physical Institute of Russian Academy of Science, Moscow, Russia.*

The search for stable heavy exotic hadrons is a promising way to observe new physics processes at collider experiments. The discovery potential for such particles can be enhanced or suppressed by their interactions with detector material. This paper describes a model for the interactions in matter of stable hadrons containing an exotic quark of charges  $\pm\frac{1}{3}e$  or  $\pm\frac{2}{3}e$  using Regge phenomenology and the Quark Gluon String Model. The influence of such interactions on searches at the LHC is also discussed.

## 1 Introduction

Searches for slow-moving stable<sup>1</sup> massive particles (SMPs) which interact within a detector offer a promising means of observing new physics processes at colliders. Their strong production mechanisms will allow hadronic SMPs to be among the exotica for which the LHC can open a discovery window for comparatively small amounts of integrated luminosity ( $\sim 1\text{fb}^{-1}$ ) [1]. The hierarchy problem suggests the manifestation of hitherto unobserved physics processes at TeV collision energies, and it is thus prudent to consider the possibility of heavy exotic stable quarks. Furthermore, such particles are predictions of phenomenological implementations of a number of candidate theories which extend the Standard Model (SM), such as supersymmetry and universal extra dimensions [1, 2, 3, 4, 5, 6]. An important uncertainty affecting the accuracy of any searches is the degree to which the detector interactions of hadronic SMPs can be modelled. In this paper a model is presented for the scattering in matter of generic heavy hadrons containing either up-like or down-like exotic quarks with charges  $\pm\frac{2}{3}e$  and  $\pm\frac{1}{3}e$ , respectively. The model is based on Regge phenomenology [7] and the Quark Gluon String Model (QGSM) [8].

Collider searches have already ruled out the direct pair production of a range of SMPs of masses up to around 200 GeV [1]. The LHC will open a new discovery window for SMPs with masses up to several TeV. The ATLAS and CMS experiments have already developed early SMP search strategies (see, for example, Refs. [9, 10, 11]), which usually require a track associated with a slow penetrating particle. To estimate the efficiency of such a search requires an understanding of the processes by which a SMP will interact with detector material. In the case of exotic heavy leptons, only electromagnetic energy loss could be expected. Hadronic SMPs could, however, also interact strongly, leading to additional energy loss and larger rates of SMPs stopped in detector material. Furthermore, hadronic SMPs could undergo charge exchange reactions, which could lead to event

---

<sup>1</sup>The term stable is taken to mean that the particle will not decay during its traversal of a detector.

topologies in which the exotic hadron appears to possess varying values of electric charge during its passage through the detector. Models of the interactions which a SMP may undergo are thus necessary in order to devise effective search strategies which can not only suppress SM background but also allow SMPs possessing different quantum numbers to be experimentally distinguished.

While the electromagnetic interactions of massive objects are well understood [12], it is uncertain how hadronic interactions of an exotic hadron should be treated. Several models of varying sophistication have been proposed for the scattering of hadrons which comprise an exotic colour octet, eg gluino [13, 14, 15, 16]. There is so far only one detailed model [15, 16] of energy loss and charge exchange associated with the scattering of heavy hadrons containing exotic quarks. This approach, implemented within GEANT [17], used a black disk approximation to obtain the total cross section and phase space arguments to predict the different types of reactions. By using Regge phenomenology and the QGSM we present in this work a complementary model which can also be included in GEANT to aid future searches.

This paper is organised as follows. The mass spectra of hadrons containing quarks and generic features of their scattering processes in matter are discussed. The QGSM and Regge-phenomenology are then used to provide a parameterisation in terms of relevant kinematic variables of single inclusive particle production arising from exotic hadron-nucleon scattering. This is used to estimate the average energy loss in such collisions and the expected rates of charge and baryon exchange processes. Using an ansatz of stable fourth generation quarks, we then describe the impact of this work on the prospects for detecting exotic hadrons at the LHC.

## 2 Properties of exotic hadrons

When considering interactions with matter, it is important to know the mass hierarchy of exotic heavy hadrons (hereafter referred to as  $H$ -hadrons). This determines the states to which a  $H$ -hadron, produced either in the primary interaction or after scattering with matter, would rapidly decay. Here, we consider only the lowest lying hadronic states, formed with an exotic heavy colour triplet charged object  $Q$  and light  $u$  and  $d$  quarks<sup>2</sup>.

As outlined in [3, 15], the lowest lying neutral and charged mesonic states should be stable since the mass difference between them is expected to be far smaller than the pion mass.

The baryon mass spectra, however, are more complicated [15]. The baryon state  $Qud$  containing light diquark system of spin 0 is the lowest lying state  $H_{Qud}$  with the other states  $H_{Quu}$  and  $H_{Qdd}$  forbidden due to the requirement of anti-symmetric baryon wave function. The heavier states with diquark spin 1 ( $H_{Qud}$ ,  $H_{Qdd}$ , and  $H_{Quu}$ ) are, however, all possible. In an analagous way to the charm sector in which the  $\Sigma_c^{0,+;++}$  decays strongly to the  $\Lambda_c$  baryon [12], it would thus be expected that any produced heavy baryons would decay to the low mass state  $H_{Qud}$  via pion emission. This state would thus be charged (neutral) for  $H$ -hadrons consisting of up-like (down-like) exotic quarks. As is shown in

---

<sup>2</sup>Unless stated otherwise, charge conjugate states are also implied throughout this paper.

Section 4, this difference in charge of the stable  $H$ -baryon has a large impact on the observable rates of  $H$ -hadrons at the LHC.

In advance of a discovery it is premature to attempt to calculate precisely the rate and mass of each species of exotic hadron. Here, it is assumed that  $H$ -hadrons are degenerate in mass and that a sample of stable  $H$ -hadrons formed in high energy collisions, such as at the LHC, comprise 90% mesons, divided equally between charged and uncharged states, and 10% baryons.

### 3 Interactions of $H$ -Hadrons in Matter

Although phenomenological models of the type presented in this work are needed to predict some of the fine details of exotic hadron interactions in matter, it is nevertheless possible to build up a qualitative picture of the scattering process [15, 18]. Owing to the size of its wavelength, the heavy exotic quark will be a spectator, and it is the low energy light quark system which interacts. Thus Regge phenomenology and the QGSM [8, 19] can be employed to model the interactions of exotic hadrons in matter.

The QGSM is based on the  $1/N_C$  expansion in QCD [20, 21] and partonic interpretation of reggeon diagrams. All QCD diagrams are classified according to their topology. In this approach one can distinguish two classes of scattering processes: reactions mediated by (a) reggeon and corresponding to planar QCD diagrams and (b) pomeron exchange related to the cylinder-type diagrams in elastic scattering. Exotic hadrons containing a light constituent anti-quark, such as a  $H_{Q\bar{q}}$  or a  $H_{Q\bar{q}\bar{q}}$  interact via pomeron and reggeon exchanges, the latter processes being due to the annihilation of light antiquarks with the quarks of detector matter. Conversely, hadrons containing a light constituent quark ( $H_{Qq}$ ,  $H_{Qqq}$ ) can only interact via pomeron exchange. Multiparticle production related to reggeon and pomeron exchange processes are shown in Fig. 1.

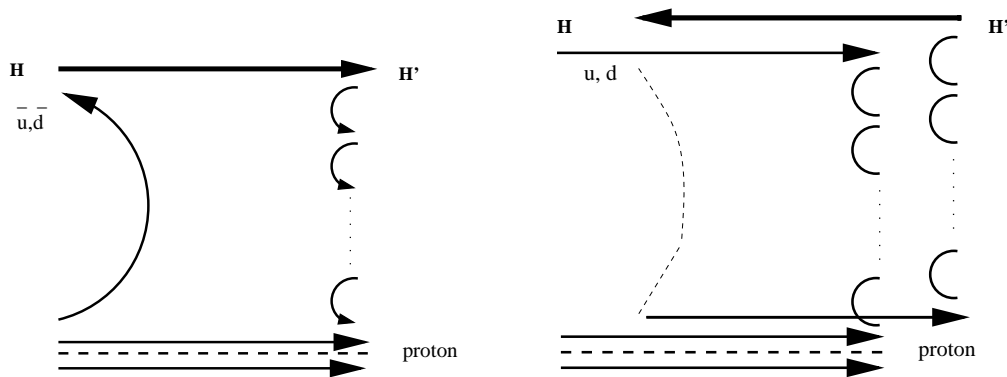


Figure 1: Diagrams representing reggeon (left) and pomeron (right) exchange between a  $H$ -hadron and a proton.

### 3.1 Total Cross Section of $H$ -hadron Scattering

Let us consider the process of an interaction of a  $H$ -hadron with a nucleon of the target nucleus in the target rest frame. In this frame the light antiquark of a  $H$ -hadron carries only a small fraction of the total energy  $E$

$$E_q \approx \frac{Em_{q\perp}}{M_H} = \gamma m_{q\perp} \quad (1)$$

where  $\gamma = E/M_H$  and  $m_{q\perp}$  is the transverse mass of the light antiquark. It was shown in the framework of the QGSM [8], that the planar diagram contribution to the total cross section  $\sigma_R(s)$  is universal for the same energy of the annihilating antiquark. This implies that the contribution to the total reggeon cross section ( $\sigma_R(E)$ ) can be written as:

$$\sigma_R(E) = K\sigma_{pl}(E = \gamma m_{q\perp}) = Kg_R(2\gamma m_{q\perp}/E_0)^{\alpha_R(0)-1} \quad (2)$$

where  $K$  is the number of possible planar diagrams and  $E_0 = 1$  GeV. The vertex parameter  $g_R$  can be evaluated from the data on cross sections of hadronic interactions [22], and the intercept of the exchange degenerate Regge trajectories  $\alpha_R(0)$  is equal to 0.5.

The pomeron contribution to the total cross section can be estimated with two models. In the additive quark model the P-contribution for the exotic meson is two times smaller than the corresponding value for pion-nucleon scattering since only one light quark (antiquark) is present. In the models in which hadrons are considered as colour dipoles the pomeron cross section is determined by the square of sizes of colliding hadrons. The mean radius squared  $r^2$  of a hadron containing one heavy and one light quark is about 1/2 of  $r^2$  of a hadron made of two light quarks and we get the same estimate for P-contribution as for the additive quark model. The pomeron cross section ( $\sigma_P$ ) depends on energy as

$$\sigma_P \sim (2\gamma m_{q\perp}/E_0)^{\alpha_P(0)-1} \quad (3)$$

The reggeon contribution to the cross section for a  $H$ -meson and a nucleon within a nucleus, which consists of equal amounts of protons and neutrons, can be derived as the difference between the reggeon contributions to  $\sigma(\pi^-p)$  and  $\sigma(\pi^+p)$  data [7] multiplied with a factor 1.5.

Fig. 2 shows the expected cross section for an exotic meson scattering off a stationary nucleon in a nucleus comprising equal amounts of protons and neutrons as a function of the Lorentz factor  $\gamma$  of the exotic hadron. The contributions from reggeon and pomeron exchange processes are shown.

Anti-baryons and baryons may interact via both reggeon and pomeron exchange, and pomeron exchange only processes, respectively. To obtain the overall cross sections for interactions involving baryons and anti-baryons, the pomeron contribution to the meson cross sections shown in Fig. 2 is doubled to take into account the extra light quark contribution. The reggeon contribution to anti-baryon scattering is taken to be twice the value for meson scattering with an added contribution from processes in which exotic anti-baryons can annihilate to exotic mesons and ordinary mesons. In the QGSM this process is described by planar diagrams with the annihilation of diquarks and string-junctions [23]. At large gamma the last process of string-junction annihilation dominates. In the

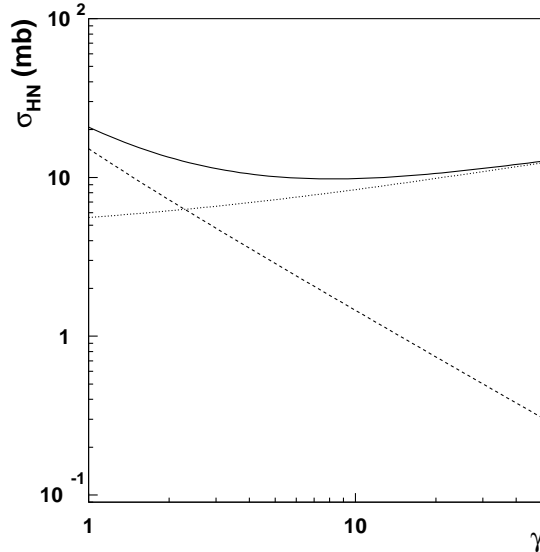


Figure 2: Pomeron (dashed) and reggeon (dotted) contributions to the exotic-meson-nucleon cross section. The sum of the two processes is shown as a solid line.

same way as for usual annihilation it will decrease with energy as  $\sim 1/\gamma^{\frac{1}{2}}$ . At  $\gamma \sim 1$  the annihilation cross section can be large ( $\sim 30$  mb), and the annihilation cross section is thus taken to be  $30\gamma^{-\frac{1}{2}}$  mb here.

An exotic baryon can convert into an exotic meson in one of the sheets of the cylinder diagram of Fig.2. This process can however be suppressed at energies close to threshold [10] by phase space effects and the absence of available pions within the nucleus which would be needed for reactions in which exotic baryons become mesons.

The Regge approach is valid for  $\gamma \gg 1$ , however it is known from experience with hadronic interactions that the Regge description works reasonably well on average for values of  $\gamma \sim 1$  [7]. The  $H$ -hadron nucleon scattering cross section ( $\sigma_{HN}$ ) is used to estimate the cross section for the interaction of a  $H$ -hadron with a nucleus of atomic number  $A$  through  $\sigma_{HA} = 1.25\sigma_{HN}A^{0.7}$  [17].

Fig. 3 shows the predicted distribution  $\frac{1}{N} \frac{dn}{d\gamma}$  of the Lorentz factor for fourth generation quarks pair produced at the LHC, as calculated by PYTHIA [24]. Here  $N$  is the total number of  $H$ -hadrons for each mass point: 200, 500, and 1000 GeV. As can be seen, for increasing mass the quarks will typically be produced with progressively smaller speeds. It should also be noted that a produced  $H$ -hadron must possess a speed above a certain threshold (for ATLAS this is conservatively estimated as  $\gamma \gtrsim 1.4$  [10]) to satisfy timing requirements for the particle to be triggered, read-out, and assigned to the correct bunch crossing.

### 3.2 Differential Cross Sections and Energy losses

In determining the kinematics of the scattering process, we consider the inclusive process  $H + N \rightarrow H' + X$ , where  $H$ ,  $H'$ ,  $N$  and  $X$  are the incoming exotic hadron, the outgoing

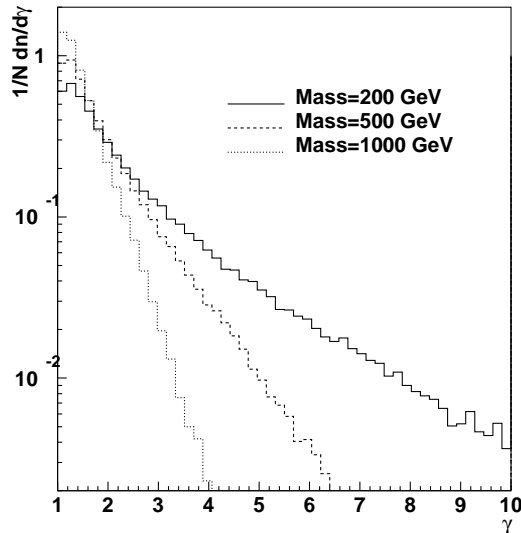


Figure 3: The distribution of the Lorentz factor  $\gamma$  of fourth generation quarks pair produced at the LHC, as predicted by PYTHIA. The spectra are shown for quark masses: 200, 500 and 1000 GeV.

exotic hadron, the target nucleon, and whatever else is produced in the interaction, respectively. The kinematics of such an interaction can be specified by three independent kinematic variables. Commonly used variables are  $t$ , the usual four-momentum transfer between the incoming and outgoing exotic hadrons,  $s$ , the squared center-of-mass energy of the interaction, and  $M_X$ , the mass of the final state  $X$ .

The final  $H'$ -hadron carries a fraction of energy  $x_F$  close to unity and only a small fraction of energy  $1 - x_F \sim m_{q\perp}/M_H \ll 1$  is transferred to production of hadrons. This justifies the application of the triple-regge formulae to provide a description of inclusive cross sections. Strictly speaking the triple-regge description is valid for  $m_X^2 \gg 1\text{GeV}^2$  and the rapidity difference between  $H'$  and rest hadrons  $\Delta y > 1$ . This is equivalent to the condition  $2\gamma m_{q\perp} m_N / M_X^2 \gg 1$ . In hadronic interactions, the triple-regge description works usually up to  $\Delta y \sim 1$  and we will assume in the following that the same is true for interaction of  $H$ -hadrons [7]. A representation of rapidity gaps between the quark systems in the three reggeon exchange diagram is shown in Fig. 4.

Expressions for the contributions of different triple-regge terms  $ik$  (Fig. 4) to inclusive cross sections is straightforward to obtain, noting that for reggeons  $i$  corresponds the factor  $\exp(2(\alpha_i(t) - 1)\Delta y)$ , while an exchange by the reggeon  $k$  leads to the factor  $\exp((\alpha_k(0) - 1)y_q)$ . Here,  $y_q = \ln(M_X^2/(m_{q\perp} m_N))$  is the rapidity interval covered by produced hadrons (the total rapidity  $Y = \ln(2E/M_H) = \ln(2\gamma) = \Delta y + y_q$ ). As for the total cross section we consider as exchanged reggeons  $i, k$  the pomeron  $P$  and secondary reggeons  $R$ . Thus we have the following triple-regge contributions:  $RRR, RRP, PPR$  and  $PPP$ .

Using the rules described above we can write inclusive cross sections for the corre-

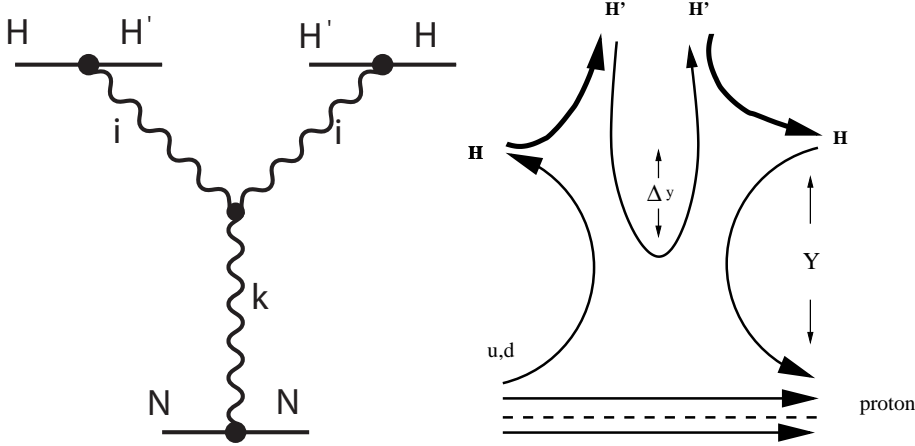


Figure 4: Left: triple-regge diagram describing the process  $H + N \rightarrow H' + X$ . Right: representation of rapidity gaps between the quark systems in the three reggeon exchange diagram.

spending triple-regge terms in the following forms:

$$\frac{d^2\sigma_{RRR}}{dt dM_X^2}(\gamma, M_X^2) = \frac{1}{M_X^2} \sigma_R^2(\gamma) C_{RRR} \exp[(2B_{RH} + B_{RRR} + 2\alpha'_R \ln(\frac{2\gamma M_0^2}{M_X^2}))t] \left(\frac{M_0^2}{M_X^2}\right)^{\Delta_R} \quad (4)$$

$$\frac{d^2\sigma_{RRP}}{dt dM_X^2}(\gamma, M_X^2) = \frac{1}{M_X^2} \sigma_R^2(\gamma) C_{RRP} \exp[(2B_{RH} + B_{RRP} + 2\alpha'_P \ln(\frac{2\gamma M_0^2}{M_X^2}))t] \left(\frac{M_0^2}{M_X^2}\right)^{2\Delta_R - \Delta_P} \quad (5)$$

$$\frac{d^2\sigma_{PPR}}{dt dM_X^2}(\gamma, M_X^2) = \frac{11}{M_X^2} \sigma_P^2(\gamma) C_{PPR} \exp[(2B_{PH} + B_{PPR} + 2\alpha'_P \ln(\frac{2\gamma M_0^2}{M_X^2}))t] \left(\frac{M_0^2}{M_X^2}\right)^{2\Delta_P - \Delta_R} \quad (6)$$

$$\frac{d^2\sigma_{PPP}}{dt dM_X^2}(\gamma, M_X^2) = \frac{1}{M_X^2} \sigma_P^2(\gamma) C_{PPP} \exp[(2B_{PH} + B_{PPP} + 2\alpha'_P \ln(\frac{2\gamma M_0^2}{M_X^2}))t] \left(\frac{M_0^2}{M_X^2}\right)^{\Delta_P} \quad (7)$$

where  $\Delta_R = \alpha_R(0) - 1 = -0.5$ ,  $\Delta_P = \alpha_P(0) - 1 = 0.12$ ,  $\alpha'_R = 0.9 \text{ GeV}^{-2}$ ,  $\alpha'_P = 0.25 \text{ GeV}^{-2}$  [8] and  $M_0^2 = m_N m_{q\perp} = 0.5 \text{ GeV}^2$ .

The parameters,  $C_{ij}$ , and  $B_{ij}$  can be determined using Regge factorization from the triple-regge description of inclusive spectra in high-energy hadronic interactions [19]. Let us emphasise that the RRR-term corresponds to the diagram of Fig. 1 (left), which represents the cutting of the planar diagram or R-exchange, while the RRP-term corresponds to the cutting of the cylinder-type diagram in Fig. 1 (right). Due to conservation of  $H$ -hadrons integrals over  $M_X^2$  and  $t$  give  $\sigma_R$  and  $\sigma_P$  contributions to the total cross section correspondingly.

The PPR and PPP-terms describe the diffractive dissociation of a nucleon and their cross sections can be calculated, using factorization from the corresponding cross sections extracted from  $pp$ -interactions

$$\sigma_{Hp}^{PPi} = \frac{\sigma_P(Hp)^2}{\sigma_P(pp)^2} \sigma_{pp}^{PPi} \quad (8)$$

Here, we neglected the small difference in  $t$ -dependence for  $Hp$  and  $PP$  vertices. Taking into account that  $\frac{\sigma_P(Hp)}{\sigma_P(pp)} \approx 1/4$  and that the sum of PPR and PPP-contributions for  $pp$ -collisions in the relevant energy domain does not exceed 2mb, we obtain very small cross sections for diffraction dissociation of a nucleon in  $Hp$ -interactions: 0.12 mb. Thus these cross sections constitute only about 1% of the total cross section and can be safely neglected in our estimates of energy losses.

For parameters characterising the  $t$ -dependence of RRR and RRP-terms we take the same values as have been extracted from analysis of  $pp$ -interactions [19]:  $2B_{RH} + B_{RRR} = 2B_{RH} + B_{RRP} = 4 \text{ GeV}^{-2}$

The energy loss of a  $H$ -hadron is given by:

$$\Delta E = \frac{M_X^2 - m_N^2 + |t|}{2m_N} \quad (9)$$

The average energy loss can thus be calculated:

$$\langle E \rangle = \frac{\int_{m_N+m_\pi}^{M_{Xmax}} dM_X \int_{|t|_{min}}^{|t|_{max}} d|t| \Delta E \frac{d^2\sigma}{d|t|dM_X}}{\int_{m_N+m_\pi}^{M_{Xmax}} dM_X \int_{|t|_{min}}^{|t|_{max}} d|t| \frac{d^2\sigma}{d|t|dM_X}} \quad (10)$$

Here,  $m_N$  and  $m_\pi$  were taken as the mass of the proton and a charge pion, respectively.

The upper limit on  $M_X$  is taken to be the lower of the following two limits:  $M_{Xmax} = (2\gamma M_0^2)^{\frac{1}{2}}$ , which represents the condition  $\Delta y = 0$  or  $M_{Xmax} = \sqrt{s} - m_H$  from energy-momentum conservation and where  $m_H$  is the mass of the interacting  $H$ -hadron.

The limits on  $t$  are given by

$$|t|_{min,max}(M_X) = 2[E(m_N)E(M_X) \mp p(m_n)p(M_X) - m_H^2] \quad (11)$$

where  $E(m) = \frac{s+m_H^2-m^2}{2\sqrt{s}}$ ,  $p(m) = \frac{\lambda^{\frac{1}{2}}(s,m_H^2,m^2)}{2\sqrt{s}}$ , and  $\lambda(a,b,c) = a^2 + b^2 + c^2 - 2(ab + ac + bc)$ .

Fig. 5 shows the mean energy loss associated with two triple-regge contributions (RRR, RRP) as a function of  $\gamma$ . The two contributions give similar values except at the very highest values of  $\gamma$ , at which the production cross section for  $H$ -hadrons is tiny. It was also found that the energy loss at a fixed  $\beta$  is insensitive to the  $H$ -hadron mass for mass values greater than around 10 GeV. The principal uncertainty in the total energy loss comes from the uncertainty in the value of  $m_{q\perp}$ , which enters via the parameter  $M_0^2$  and was chosen to be  $0.5 \text{ GeV}^2$  for this work. Taking values of  $M_0^2$  of 0.3 or  $0.7 \text{ GeV}^2$  changes the average energy values typically by around 50% and this would not change the conclusions of this paper.

For calculations of energy losses of a given  $H$ -hadron type we need in principle to know only the losses associated with each triple-regge term and the relative weights of different terms. For RRR and RRP-terms these weights are given by  $\sigma_R(\gamma)/\sigma^{tot}(\gamma)$  and  $\sigma_P(\gamma)/\sigma^{tot}(\gamma)$  correspondingly. However, since the difference in energy loss from the two contributions is anyway very small,  $H$ -hadron energy loss for both reggeon and pomeron interactions was assumed to be that given by the RRP term.

A Monte Carlo method was used to extract the predicted distributions  $f(E) = \frac{1}{N} \frac{dn}{dE}$  of energy loss ( $E$ ) at a range of values of  $\beta$ , where  $N$  is the total number of  $H$ -hadrons



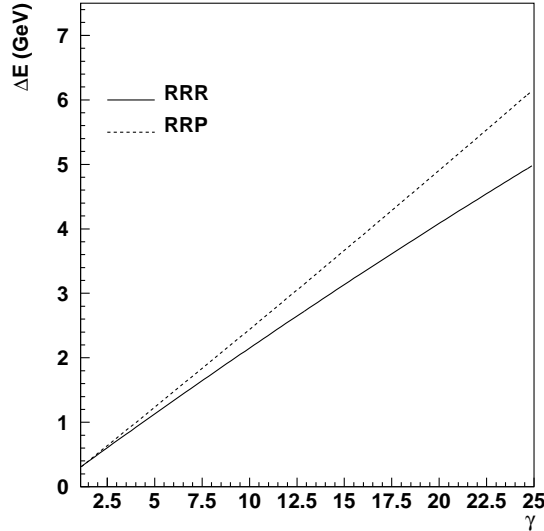


Figure 5: Average energy loss per interaction as a function of  $\gamma$  for two triple-regge terms.

at each  $\beta$  point. The functional form  $f(E)$  for RRR and RRP terms in the  $H$ -hadron  $\gamma$  range expected at the LHC ( $\gamma \lesssim 10$ ) can be approximated by Equation 12.

$$f(E) = \exp[-10(E - 0.3)^2(1 - \beta)^{1.5}] \frac{1.0}{1 + (\frac{0.3}{E})^{15}} \quad (12)$$

This function was used to arrive at the results presented in Section 4. Fig. 6 shows  $f(E)$  for an exotic  $H$ -hadron of mass 200 GeV for four values of  $\beta$ . The distribution typically extends up to around a few GeV, though it is peaked at around 0.5 GeV.

### 3.3 Charge Exchange and Baryon Formation

Charge exchange processes will naturally take place via the formation of light quark pairs from the vacuum both for planar (Fig.1) and cylinder-type (Fig.2) diagrams. As  $u$  and  $d$  quarks are produced with equal probability we expect that charge exchange happens with 50% probability per interaction.

Within the Lund string model [25] exotic baryons only account for around 10% of all exotic hadrons produced at the primary interaction, a prediction which is also made in the QGSM [26]. Baryons can also be produced as a result of hadronic interactions of exotic mesons in matter. The probability that a given inelastic collision involving an exotic meson results in baryon formation takes place is taken to be 10%, a value motivated by investigation of baryon production in QGSM and low energy hadron scattering data [8]. The proportion of different baryon species formed in such interactions is taken to be the same as at the primary interaction.

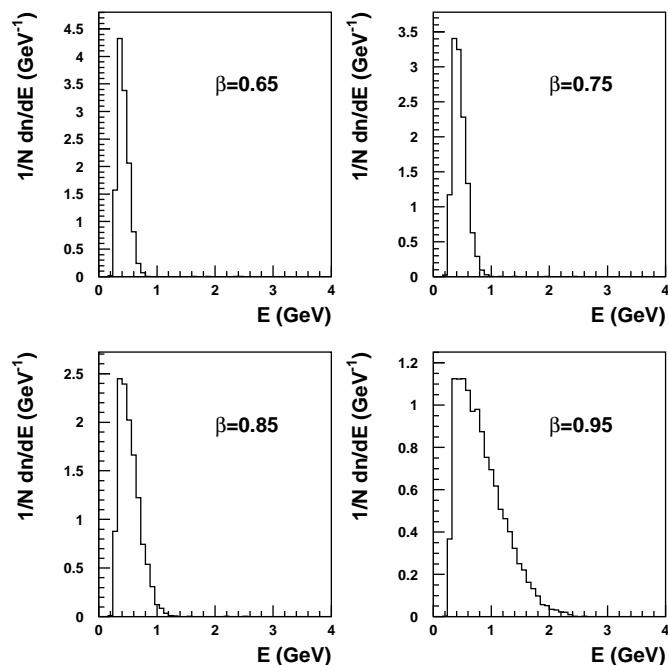


Figure 6: The predicted distribution  $\frac{1}{N} \frac{dn}{dE}$  of the energy loss per interaction of a  $H$ -hadron of mass 200 GeV and for different values of  $\beta$ .

## 4 Experimental Signatures

In this section the model of hadronic scattering outlined in Section 3, together with the well established theory of electromagnetic energy loss of charged particles in matter [12], is used to estimate the energy losses and rate of charge exchange reactions of a  $H$ -hadron propagating through the ATLAS detector [27] at the LHC. Calculations of the cross section for fourth generation quark pair production at the LHC are then used to predict the rates of various event topologies associated with  $H$ -hadron production. The event topologies are characterised by the values of charges possessed by the  $H$ -hadrons in the inner and muon tracking chambers, i.e. before and after scattering in the ATLAS calorimeter system.

### 4.1 Energy Loss and Charge Exchange

To estimate the kinematic distributions of  $H$ -hadrons produced at the LHC, the PYTHIA [24] program was used to generate samples of 50,000 fourth generation quark pair production events for quark masses 200, 500 and 1000 GeV. It was assumed that the proportion of different types of stable  $H$ -hadrons formed from these quarks follows the prescription given in Section 2. To ensure that  $H$ -hadrons would belong to a high acceptance region of the ATLAS detector, the initial value of  $\beta$  of the  $H$ -hadrons was required to be

greater than 0.7 and the pseudorapidity was restricted to  $|\eta| < 2.5$  [10]. The remaining  $H$ -hadrons were then transported, using a Monte Carlo method, through material of thickness corresponding to the part of the ATLAS detector enclosed by the muon tracking chamber.

The material distribution of the sub-systems of the ATLAS detector enclosed by the muon detector varies between around 11 and 19 interaction lengths as a function of pseudorapidity [27]. The largest material contribution ( $\sim 70\%$  of the total thickness) arises from the absorbing material in the different hadronic calorimeter systems. These systems are the Tile Calorimeter (TileCal) [28] and Hadronic EndCap Calorimeter (HEC) [29], which use iron and copper, respectively, as absorbers. Thus, for a generated  $H$ -hadron falling in the pseudorapidity regions  $|\eta| < 1.5$  ( $1.5 < |\eta| < 2.5$ ) covered by the TileCal (HEC), iron (copper) was used to represent the ATLAS detector material in the Monte Carlo calculations presented here.

Fig. 7 shows differential distributions related to the energy loss and interactions of  $H$ -hadrons as they pass through the detector material. Spectra are shown separately for  $H$ -hadrons formed from different types of exotic quarks and anti-quarks with masses 200 and 1000 GeV. The distributions are normalised to the total number  $N$  of a given type of  $H$ -hadron satisfying the  $\beta$  and  $\eta$  requirements. In the following discussion of the plots  $H_Q(H_{\bar{Q}})$  is used as a generic term to denote a  $H$ -hadron with an exotic quark (anti-quark) while the terms  $H_U, H_D, H_{\bar{U}},$  and  $H_{\bar{D}}$  are used to denote  $H$ -hadrons with up-like and down-like exotic quarks and anti-quarks.

The distributions of total energy loss are peaked at  $\sim 4$ -5 GeV and extend up to around 10 GeV for the different  $H$ -hadron types, with no substantial mass dependence. The  $H_D$ -hadrons typically show lower energies than the  $H_U$ -hadrons. This is due to differences in ionisation energy loss since  $H_D$ -hadrons are more likely to propagate through the material with zero electric charge. A  $H_D$ -hadron can, for example, start as a neutral meson and then be converted into a neutral baryon. The effect can be seen as a peak at low ionisation energy loss for  $H_D$ -hadrons. Smaller peaks at low ionisation energy loss are also visible for the  $H_{\bar{Q}}$ -hadrons, which arise from events in which those  $H$ -hadrons propagate through the material mostly as neutral mesons.

The hadronic energy loss for the  $H$ -hadrons decreases slightly with mass owing to the typically lower speeds of the more massive  $H$ -hadrons (see Fig. 5). The hadronic energy loss for  $H_Q$ -hadrons peaks at around 3-4 GeV, which is larger than that for  $H_{\bar{Q}}$ -hadrons ( $\sim 1$  GeV). This can be understood as a consequence of the different reaction channels, which are open for  $H_Q$  and  $H_{\bar{Q}}$ -hadrons.  $H$ -hadrons are dominantly mesonic following hadronisation and, although they can form baryons, still interact mostly as mesons. As explained in Section 3,  $H_Q$ -mesons may scatter via reggeon or pomeron exchange, unlike  $H_{\bar{Q}}$ -mesons, which interact with a lower cross-section since only pomeron exchange is possible in this case. This is seen in the distribution of the multiplicity of hadronic interactions, which peaks at  $\sim 5$  ( $\sim 2$ ) for  $H$ -hadrons with exotic quarks (anti-quarks).

Within the  $H$ -hadron kinematic region under study, the stopping of  $H$ -hadrons is negligible, as can be understood from their low energy losses. The decrease in speed  $\delta\beta$  of a  $H$ -hadron following the traversal of detector material in the ATLAS detector was calculated and it was found that  $\delta\beta \lesssim 0.005$  ( $\delta\beta \lesssim 0.02$ ) for a mass of 200 GeV (1000 GeV).

The results given above were obtained assuming that a neutral  $H$ -hadrons could not

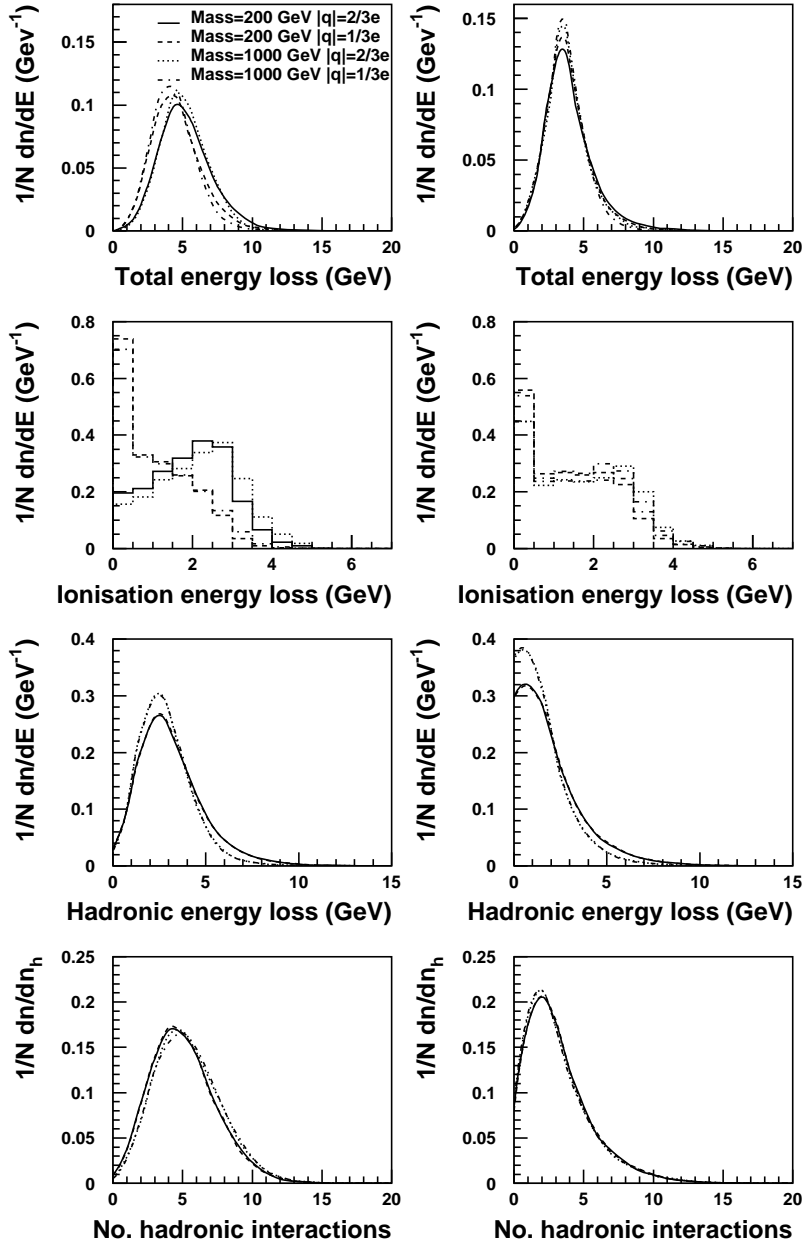


Figure 7: Distributions of energy loss and hadronic scattering for  $H$ -hadrons of masses 200 and 1000 GeV and for exotic quarks of charges  $\pm\frac{1}{3}e$  and  $\pm\frac{2}{3}e$ . The left (right) column represents  $H$ -hadrons containing an exotic quark (anti-quark). Distributions of the total, ionisation and hadronic energy loss is shown along with the multiplicity of interactions. The distributions assume no mixing of neutral  $H$ -mesons.

oscillate into its anti-particle, something which has been studied in the context of supersymmetry [3, 30]. In a strictly generic scenario of new physics, as considered here, it is prudent to consider the possibility of two extreme cases: maximal and no mixing. Allowing maximal mixing produces distributions (not shown), which are very similar to those given in Fig. 7. However, together with the effects of hadronisation and scattering interactions it can give rise to striking event topologies, which can be used to detect and characterise  $H$ -hadron, as is shown in Section 4.2.

## 4.2 Expected Rates of $H$ -hadrons

Fig. 8 shows the expected cross section for the pair production of fourth generation quarks of a single flavour at the LHC, as predicted by PYTHIA. The cross section is seen to fall steeply with mass. Nevertheless, for a full year's LHC running at low luminosity, corresponding to  $10 \text{ fb}^{-1}$ , around 25,000 pairs would still be expected for a 500 GeV mass, implying that exotic hadrons can be sought with early LHC data.

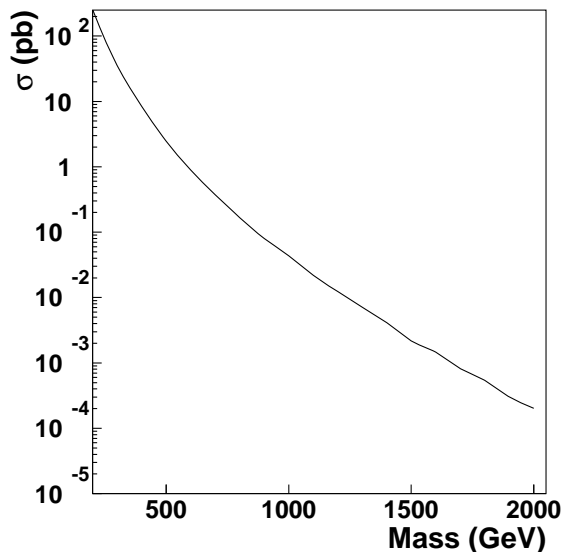


Figure 8: Predicted cross section, calculated to leading order, for the pair production of fourth generation quarks at the LHC.

Following the acceptance cuts and  $H$ -hadron transport through ATLAS described in Section 4.1, Tabs. 1 and 2 contain the expected yields for a range of event topologies arising from the pair production of exotic quarks possessing  $\pm\frac{1}{3}e$  and  $\pm\frac{2}{3}e$ . Rates are shown for  $H$ -hadrons of mass 200, 500 and 1000 GeV and an integrated luminosity of  $10 \text{ fb}^{-1}$  is assumed. The topologies are:

1. At least one  $H$ -hadron is produced with non-zero charge and retains that charge value throughout its passage in the detector material implying that the inner and muon tracking chambers measure the same charge;

2. Both particles are produced with non-zero charge and retain those charge values.
3. Both particles are produced with non-zero charge and one retains its non-zero charge but the other is converted into a neutral state.
4. One particle is produced with zero charge whilst the other has non-zero charge; the particle produced with zero charge converts into a charged state whilst the other retains its original value of charge.
5. Both particles are produced with non-zero charge but leave the detector material as neutral states.
6. At least one particle leaves the detector material possessing a non-zero electric charge of opposite sign to the charge with which it was produced.

Topology	No mixing Mass (GeV)			Maximal mixing Mass (GeV)		
	200	500	1000	200	500	1000
1	$4.9 \times 10^5$	$4.3 \times 10^3$	57	$4.1 \times 10^5$	$3.5 \times 10^3$	48
2	$3.0 \times 10^4$	$2.6 \times 10^2$	3	$2.2 \times 10^4$	$1.9 \times 10^2$	2
3	$9.6 \times 10^4$	$8.3 \times 10^2$	9	$8.2 \times 10^4$	$6.8 \times 10^2$	8
4	$6.0 \times 10^4$	$5.2 \times 10^2$	6	$4.8 \times 10^4$	$4.0 \times 10^2$	5
5	$6.4 \times 10^4$	$5.3 \times 10^2$	6	$6.3 \times 10^4$	$5.5 \times 10^2$	6
6	0	0	0	$8.1 \times 10^4$	$7.2 \times 10^2$	9

Table 1: Expected rates of various topologies, corresponding to an integrated luminosity of  $10\text{fb}^{-1}$ , for different event topologies arising from the pair-production of exotic quarks of charge  $\pm\frac{1}{3}e$ .

As can be seen, substantial rates for the mass points 200 and 500 GeV can be expected for each of the topologies. While the first two topologies offer the classic signature of a single or a pair of high momentum penetrating particles, scenarios 3 and 4 show evidence of charge exchange and can thus be used in combination with calorimeter information to identify the SMP as being hadronic and reject alternative scenarios, such as stable leptons. Scenario 5 may be the most experimentally challenging topology if a muon-based trigger is used, although, as seen, this topology accounts for only a small fraction of events. The observation of topology 6 could demonstrate mixing in the  $H$ -hadron sector.

A comparison of Tabs. 1 and 2 shows the rates for all of the considered topologies bar scenario 5 are greater for  $H$ -hadrons with up-like exotic quarks than those for those with down-like exotic quarks. However, the situation is reversed for topologies (5). This can be explained as being due to the production of baryons which have zero (non-zero) charge for  $\pm\frac{1}{3}e$  ( $\pm\frac{2}{3}e$ ) charge exotic quarks.

Topology	No mixing Mass (GeV)			Maximal mixing Mass (GeV)		
	200	500	1000	200	500	1000
1	$8.8 \times 10^5$	$8.0 \times 10^3$	107	$8.0 \times 10^5$	$7.2 \times 10^3$	97
2	$1.2 \times 10^5$	$1.0 \times 10^3$	12	$8.6 \times 10^4$	$7.7 \times 10^2$	8
3	$1.3 \times 10^5$	$1.2 \times 10^3$	13	$1.0 \times 10^5$	$8.9 \times 10^2$	10
4	$1.7 \times 10^5$	$1.5 \times 10^3$	17	$1.8 \times 10^5$	$1.5 \times 10^3$	17
5	$2.9 \times 10^4$	$2.5 \times 10^2$	3	$2.5 \times 10^4$	$2.1 \times 10^2$	2
6	0	0	0	$1.9 \times 10^5$	$1.7 \times 10^3$	23

Table 2: Expected rates of various topologies, corresponding to an integrated luminosity of  $10\text{fb}^{-1}$ , for different event topologies arising from the pair-production of exotic quarks of charge  $\pm\frac{2}{3}e$ .

### 4.3 Detector Effects

It is beyond the scope of this paper to study in detail the expected response of the ATLAS detector. Such work is more appropriately made with the ATLAS simulation and event reconstruction packages [31]. However, a few comments can be made based on earlier work employing such programs and the results presented in this Sections 4.1 and 4.2 should be considered in the light of these.

It is desirable for any search to include calorimeter information. The observation of small hadronic energy depositions associated with a penetrating SMP could be used, for example, to reject backgrounds of muons. Furthermore, as shown in Fig 7, differences in hadronic energy loss between a pair of SMP candidates could provide evidence for stable exotic quarks. To study the feasibility of exploiting calorimetry in this way, the model presented here should be implemented within a package such as GEANT in order to include effects such as nuclear fragmentation [17].

A conservative estimate of the trigger efficiency for a slow moving particle using a muon trigger of 50% has been made [10]. Therefore, with the exception of topology 5, events corresponding to the topologies listed above should be recorded in this way. It may be possible to select events corresponding to topology 5, through a jet or missing transverse energy trigger, in the case when one of exotic quarks emits a high transverse momentum quark or gluon. The track reconstruction efficiency in the inner and muon tracking chambers should be over 90% in the kinematic region under investigation [27], though further losses could occur due to charge exchange interactions of  $H$ -hadrons in the different tracking systems. More studies on efficiency losses using, for example, the model presented in this work is desirable. Furthermore, the charge misidentification probability for tracks in the muon (inner) detector should be around 2% (4%) for transverse momentum  $p_T$  values up to around 1 TeV and falls quickly with decreasing  $p_T$  [27]. While it could be expected that the charge misidentification probability may be degraded for interacting  $H$ -hadrons, earlier work with gluinos involving a full ATLAS detector simulation showed that a signature of an exotic hadron apparently reversing the sign of its charge is a useful

search observable [32]. We would thus expect topology 6 to be distinguished.

SM backgrounds can be suppressed in a number of ways, for example by making requirements on the SMP's transverse momentum ( $p_T \gtrsim 100$  GeV) and event shape variables [10, 32]. The most promising method is to use a time-of-flight technique [10] with which exotic hadron searches in early LHC data may only suffer from a handful of background events.

## 5 Conclusions

Heavy exotic quarks are predicted in a number of scenarios of physics beyond the SM. This paper presented a generic model based on Regge theory and the Quark Gluon String Model to describe the interactions of heavy hadrons in matter. The work showed how strong interactions of exotic hadrons may provide useful observable to detect and quantify the properties of any exotic stable massive particle which may be observed. Distributions relating to the interactions and estimates of expected event topologies at the LHC were shown. A natural next step in this work would be the implementation of this model within GEANT and its subsequent use in searches at colliders and studies of discovery potential.

## 6 Acknowledgements

A. Kaidalov is partially supported by the following grants from the Russian Foundation for Basic Research: RFBR 06-02-17012, RFBR 06-02-72041-MNTI, together with the Russian Scientific School Grant 843.2006.2.

D. Milstead is a Royal Swedish Academy Research Fellow supported by a grant from the Knut and Alice Wallenberg Foundation.

## References

- [1] M. Fairbairn, A. C. Kraan, D. A. Milstead, T. Sjöstrand, P. Skands and T. Sloan, *Phys. Rept.* **438** (2007) 1 [arXiv:hep-ph/0611040].
- [2] G. R. Farrar and P. Fayet, *Phys. Lett. B* **76** (1978) 575
- [3] S. J. Gates and O. Lebedev, *Phys. Lett. B* **477** (2000) 216 [arXiv:hep-ph/9912362].
- [4] M. B. Chertok, G. D. Kribs, Y. Nomura, W. Orejudos, B. Schumm and S. Su, in *Proc. of the APS/DPF/DPB Summer Study on the Future of Particle Physics (Snowmass 2001)* ed. N. Graf, *In the Proceedings of APS / DPF / DPB Summer Study on the Future of Particle Physics (Snowmass 2001), Snowmass, Colorado, 30 Jun - 21 Jul 2001, pp P310* [arXiv:hep-ph/0112001].
- [5] J. L. Diaz-Cruz, J. R. Ellis, K. A. Olive and Y. Santoso, *JHEP* **0705** (2007) 003 [arXiv:hep-ph/0701229].
- [6] S. P. Martin, *Phys. Rev. D* **75** (2007) 115005 [arXiv:hep-ph/0703097].



- [7] P.D.B. Collins, Phys. Rept. **1** (1971) 103.  
P.D.B. Collins, An Introduction to Regge Theory, Cambridge (1977).
- [8] A.B. Kaidalov, Phys. Lett. B **116** (1982) 459.  
A.B. Kaidalov and K.A. Ter-Martirosyan, Phys. Lett. **B 117** (1982) 247  
A.B. Kaidalov and K.A. Ter-Martirosyan, Sov.J.Nucl.Phys.**39**(1984)1545;  
A.B. Kaidalov and O.I. Piskounova, Sov.J.Nucl.Phys.**41**(1985)1278;  
O. Piskounova, Phys.At.Nucl. **66** (2003) 332 [arXiv:hep-ph/0202005].
- [9] S. Ambrosanio, B. Mele, A. Nisati, S. Petrarca, G. Polesello, A. Rimoldi and G. Salvini, [arXiv:hep-ph/0012192].
- [10] A. C. Kraan, J. B. Hansen and P. Nevski, Eur. Phys. J. C**49** (2007) 623 [arXiv:hep-ex/0511014].
- [11] M. Johansen, [arXiv:hep-ex/0701055].
- [12] W. M. Yao *et al.* [Particle Data Group], J. Phys. G **33**, 1 (2006).
- [13] H. Baer, K. m. Cheung and J. F. Gunion, Phys. Rev. D **59** (1999) 075002 [arXiv:hep-ph/9806361].
- [14] A. Mafi and S. Rabi, Phys. Rev. **D 62** (1999) 3.
- [15] A.C. Kraan Eur. Phys. J. **C 37** (2004) 91
- [16] R. Mackeprang and A. Rizzi, Eur. Phys. J. C **50**, 353 (2007) [arXiv:hep-ph/0612161].
- [17] GEANT - Detector description and simulation tool, CERN Program Library Write-up, W5013, CERN, Geneva, 1993.  
S. Agostinelli *et al.* [GEANT4 Collaboration], Nucl. Instrum. Meth. A **506** (2003) 250.
- [18] M. Drees and X. Tata, Phys. Lett. **B 252** (1990) 695.
- [19] A.B.Kaidalov, Phys.Rep. **50**(1979)157.
- [20] G. t'Hooft, Nucl. Phys. **B72** (1974) 461.
- [21] G. Veneziano, Phys. Lett. **B52** (1974) 220.
- [22] P.E.Volkovitski, A.B.Kaidalov, Sov. J. Nucl.Phys. 35(1982)1231.
- [23] G.C. Rossi and G. Veneziano, Nucl. Phys. **45** (1977) 507.
- [24] T. Sjöstrand *et al.*, Comput. Phys. Commun. **135** (2001) 238.
- [25] B. Andersson, G. Gustafsson, G.I. Ingelman, and T.Sjöstrand, Phys. Rep. **97** (1983) 31.
- [26] A. B. Kaidalov and O. I. Piskunova, Z. Phys. C **30** (1986) 145.

- [27] ATLAS Collaboration, *ATLAS: Detector and Physics Performance Technical Design Report*, CERN-LHCC-99-14.
- [28] P. Adragna *et al.*, IEEE Trans. Nucl. Sci. **53** (2006) 1275.
- [29] D. M. Gingrich *et al.*, JINST **2** (2007) P05005.
- [30] U. Sarid and S. D. Thomas, Phys. Rev. Lett. **85** (2000) 1178 [arXiv:hep-ph/9909349].
- [31] D. Rousseau, Eur. Phys. J. C **33** (2004) S1038.
- [32] S. Hellman, D. Milstead and M. Ramstedt, ATLAS Public Note, ATL-PHYS-PUB-2006-005.